

Determination of the inter- and intra-granular critical currents in superconducting $\text{YBa}_2\text{Cu}_3\text{O}_7$ welds

B Bozzo¹, S Iliescu¹, E Bartolomé¹, A Palau¹, X Granados¹, T Puig¹,
X Obradors¹, J Amorós² and M Carrera³

¹ Institut de Ciència dels Materials de Barcelona, Campus UAB, 08193 Bellaterra, Spain

² Departament de Matemàtica Aplicada I, UPC Diagonal, 647 Barcelona, Spain

³ Departament de Medi Ambient i Ciències del Sol, Universitat de Lleida, Jaume II, 69 25001 Lleida, Spain

Received 13 May 2005, in final form 24 June 2005

Published 3 August 2005

Online at stacks.iop.org/SUST/18/1227

Abstract

A method for determining simultaneously the inter- and intra-grain critical currents has been developed in welded $\text{YBa}_2\text{Cu}_3\text{O}_7$ (YBCO) ceramics by solving the Inverse Problem for local maps of the magnetic field in the remanent state. From that current distribution, the current density flowing through the superconducting weld as well as the current density circulating inside the grains can be deduced. The method is discussed and it is applied to several examples of YBCO/Ag/YBCO welds. The results obtained show that it is possible to obtain superconducting joints with a quality at the same level as that of the starting material.

(Some figures in this article are in colour only in the electronic version)

1. Introduction

High-quality bulk $\text{YBa}_2\text{Cu}_3\text{O}_7$ (YBCO) single domains are usually fabricated by the top-seeded melt texture growth (MTG) technique [1]. Unfortunately, the MTG process limits the shape of YBCO pieces to simply connected geometries and sizes no larger than approximately 50 mm. This introduces a limitation for application development, since in most cases pieces of complex shapes and/or large sizes are required.

In order to overcome this limitation, two main solutions have been proposed: the use of multi-seeding [2, 3], that consists of inducing the growth in several points of the sample; or welding individual melt-textured tiles. The different welding techniques developed are either based on the superheating effect [4], the use of lower-melting point superconductor matrices as welding agents like REBCO oxides ($\text{RE} = \text{Y, Yb, Er, Tm}$) [5–8] or YBCO/Ag composites [9, 10]. In a previous work, we introduced a new welding technique consisting of the use of a thin silver foil as the welding agent [11, 12].

Ideally, the aim would be that the artificially introduced joint would be able to carry a critical current density, J_c^{GB} , comparable to that of the grains, J_c^{G} , with a comparable

dependence on the applied magnetic field. So, an adequate quality parameter would be the $J_c^{\text{GB}}/J_c^{\text{G}}$ ratio. In order to obtain it, several methods have been suggested to determine the inter- and intra-grain critical current densities. Direct transport current [6, 10] and magnetoresistance [13] measurements have been performed, although the method is cumbersome and time-consuming due to the necessity of making good-quality contacts. Inductive measurements in ring-shaped samples containing joints have also been proposed [14–16]. However, due to the geometry of the samples, only a small portion of the junction (typically 1 mm^2) can be evaluated, which might not be representative of the whole welded specimen. Direct observation of the magnetic field on the surface in the remanent state could be done by magneto-optical measurements [17–19]. These allow, in principle, the characterization of the whole junction length; however, because of the saturation of the garnet films utilized, the range of applied fields is limited to a few hundreds of gauss. The visualization of the map of the trapped magnetic field by Hall probe scanning [15, 20, 21] has been the most used technique to characterize the quality of the superconducting joints. The characterization of the magnetic behaviour of superconducting welds along hysteresis cycles, measured by Hall probe scanning in field conditions up to 1 T,

has been reported [21]. However, the absolute values of the trapped fields depend on the particular geometry and size of the welded sample, and the sample-to-probe distance, making it difficult to compare the performance of different joints.

In the present contribution, we discuss a method for the simultaneous determination of J_c^{GB} and J_c^G of superconducting welded samples from Hall probe measurements. The current distribution through the sample is computed with the help of an Inverse Problem solver [22], and the obtained current density map is analysed in terms of the profile expected according to the Bean model. The methodology has been systematically applied to characterize the quality of YBCO/Ag/YBCO welds fabricated by our silver-induced surface melting technique [11], and several remarkable examples will be reported here.

2. Experimental details

The superconducting welded samples were prepared as follows. Non-oxygenated single-domain YBCO pellets ($Y_{123} + 25 \text{ mol\% } Y_2O_3 + 1 \text{ wt\% } CeO_2$) [23] of size $40 \times 40 \times 12 \text{ mm}^3$, fabricated by Nexans Superconductors GmbH, were cut into several $a \times b \times c = 10 \times 10 \times 10 \text{ mm}^3$ cubes. Each cube was cut parallel to the c -axis into two similar pieces, and the faces to be rejoined were carefully polished down to $1 \mu\text{m}$ grade. The two tiles were then tightly fixed together, with a $10 \mu\text{m}$ Ag foil sandwiched in between. The YBCO/Ag/YBCO sample was subjected to a thermal treatment consisting of heating up to a temperature between 980 and 1010 °C for 3 h, followed by a slow cooling from 980 down to 950 °C. Finally, the specimen was fast cooled to room temperature. Thereafter, the sample was annealed in flowing oxygen at 450 °C for 168–240 h and at a pressure of 1.1 bar. The T_c for the welded samples is 91 K.

The magnetic characterization of the welds was performed with an in-field Hall probe scanning system developed in our group [20, 21, 24]. The system consists of an AsGa Hall probe, with an active window of $0.1 \times 0.1 \text{ mm}^2$, attached to a raster controlled by two motors, that scans the surface of the sample at a distance of approximately 80–100 μm . Local magnetization maps $B_z(x, y) - \mu_0 H$ of surfaces as large as $50 \times 50 \text{ mm}^2$ can be measured. The spatial resolution is normally 160 μm , for which the scanning time is ~ 20 min. The spatial resolution can optionally be refined down to 32 μm . The insert is placed into a boiling nitrogen cryostat, which fits inside the gap of an electromagnet, making it possible to apply magnetic fields ranging from -1 to 1 T perpendicular to the sample surface during the measurement. The welded samples were field-cooled (FC) down to 77 K and under a magnetic field $H \parallel c$ of 0.6 T. Then, the field was removed and the remanent $B_z(x, y)$ was measured.

3. Inter- and intra-granular critical currents determination method

The methodology developed for the determination of the inter- and intra-grain critical current densities in welded samples is directly based on the analysis of the current distribution expected for a two-domain block, derived from the Bean critical state model [25], as described below.

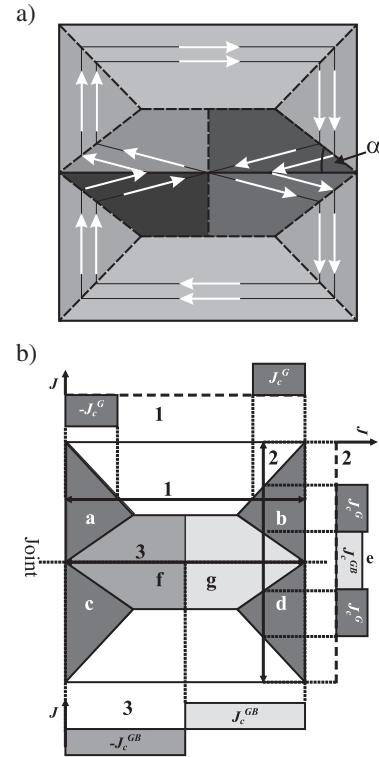


Figure 1. (a) Current lines for a bicrystal assuming the Bean model. (b) Schematic representation of the zones where the J_y is not null. The intra-grain critical current, J_c^G , can be obtained from a profile passing through the zones a and b or c and d (top). The inter-grain critical current density, J_c^{GB} , is determined by profiling on top of the junction (profile 3). That profile will pass through the zones f and g. The junction position can be easily located by identifying the lowest plateau (zone e in profile 2).

3.1. Current distribution for a two-domain block under the critical state scope

In the framework of the Bean model, which assumes that both J_c^{GB} and J_c^G are field independent, the critical state pattern of currents for a two-domain block presented in figure 1(a) can be expected. Extensive magneto-optic measurements on two-domain blocks with different grain boundary disorientation angles [17] have confirmed this pattern. The current streamlines bend at the grain boundary region with an angle α (figure 1(a)) that is related to the ratio of inter- to intra-grain critical current density as $\cos 2\alpha = J_c^{GB}/J_c^G$. In the example shown in figure 1(a), $J_c^{GB}/J_c^G = 0.25$ and $\alpha = 38^\circ$. The flux penetration through the grain boundary is faster than the penetration in the grains since the critical current density at the grain boundary is lower. When the critical current density streamlines reach the centre of the sample, closed loops are formed inside the grains. Therefore, two kind of induced current loops can be distinguished (see figure 1(a)): those extending through the whole sample, and those circulating uniquely within the grains. The formation of the two unconnected current loops depends on two parameters: the size of the two-domain block and the ratio J_c^{GB}/J_c^G .

The critical state J_c map of currents can be decomposed into its two J_x and J_y Cartesian coordinates, where the OX axis is parallel to the junction. For the determination method of J_c^G

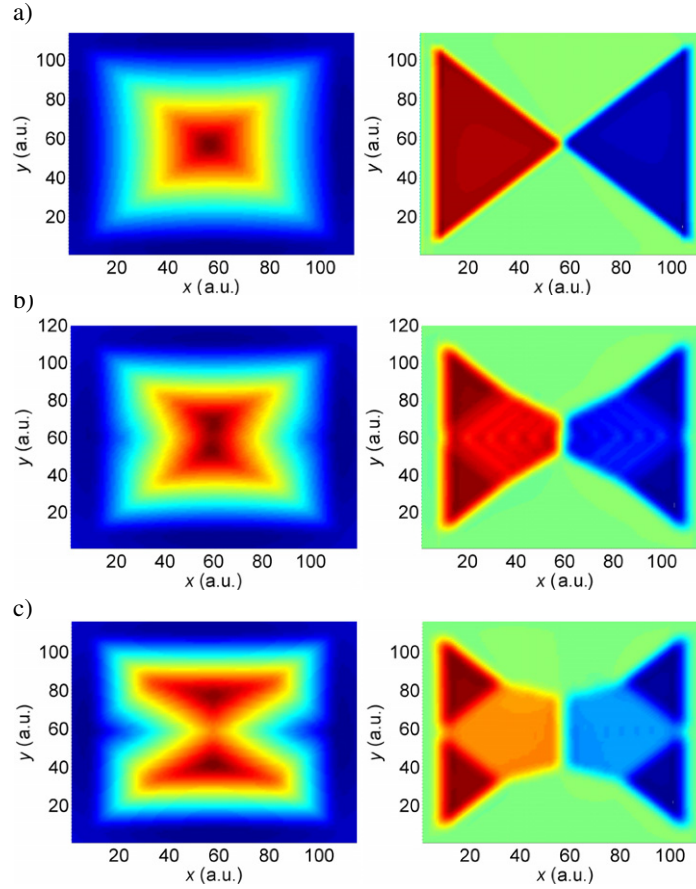


Figure 2. Modelization of three different welds with theoretical J_c^{GB}/J_c^G ratios of: (a) 100%, (b) 90% and (c) 50%. Left column: simulated magnetization maps obtained with the ‘Trazacorrientes’ program. Right column: corresponding $J_y(x, y)$ maps obtained from inversion of the left magnetization maps, using the ‘Caragol’ software.

and J_c^{GB} that we propose, it will be useful to consider only the J_y component map, as shown in figure 1(b), since we will use the component perpendicular to the junction to evaluate the inter-grain J_c^{GB} values directly. The triangles (a, b, c and d) in figure 1(b) represent the areas where J_y corresponds fully to the intra-grain J_c^G , whereas the central zones (f and g) represent the area where J_y corresponds to the J_c^{GB} . Hence, the value of J_c^G can be found by looking for the current in the triangular areas a, b, c or d shown in figure 1(b). According to the Bean model, where $|\vec{J}|$ is constant, the current along section 2 will form two peaks. The weld can be localized at the minimum of profile 2, where both J_c^{GB} and J_c^G contributions exist (figure 1(b), right). Once the position of the joint is localized, we can look for section 3, where J_y is just the critical current density at the junction, J_c^{GB} .

Hence, the analysis of the J_y component map of currents provides a simple method for the simultaneous determination of the inter- and intra-grain critical current densities.

3.2. Influence of the J_c^{GB}/J_c^G ratio on the trapped field shape

It is interesting to study theoretically the influence of the J_c^{GB}/J_c^G ratio on the shape of the $B_z(x, y)$. In order to do so, we modelled the case of three superconducting welds having J_c^{GB}/J_c^G ratios of 100%, 90% and 50%, and simulated

the induced current pattern with the help of a self-developed software called ‘Trazacorrientes’ [26]. Basically, the program, described in more detail in [26, 27], builds up the structure of shielding currents for a superconductor containing any given distribution of non-superconducting inhomogeneities, on the basis of the Bean model critical state in a 2D symmetry.

The superconducting space is modelled on an $n \times m$ bitmap of the sample, where each pixel assumes a value according to the state of the corresponding state in the superconducting sample. At the start point of the simulation, when the applied magnetic field is zero, the value of each pixel is either 0 or -1 , with 0 meaning that the site is eligible to transport an elemental current loop, and -1 representing any non-superconducting defect in the sample.

In the present case, the simulated superconducting space was a 100×100 bitmap filled with ‘zeros’, split by an alternating queue of -1 and 0 valued pixels simulating the junction. The J_c^{GB}/J_c^G ratio would thus be varied by tuning the distance between such pixels.

Once the current pattern has been simulated, the $B_z(x, y)$ map is calculated. Figure 2 shows the remanent field map calculated for the three simulated cases: $J_c^{GB}/J_c^G = 100\%$, 90% and 50%. As expected, for the 100% in ratio, the field profile consists of only a single peak (figure 2(a), left). For the 90% and 50% ratios, however, the depression of

the superconducting properties is clearly appreciated by the presence of two peaks instead of one, even though the ratio remains acceptably high. This proves that the shape of the field profile is very sensitive to the presence of defects at the junction and the presence of two peaks does not necessarily indicate an unsuccessfully welded sample.

Usually, the situation encountered is the opposite: the $B_z(x, y)$ is known from measurements, and the current density pattern must be inferred by back-solving the Biot–Savart law

$$\vec{B}(\vec{r}) = \frac{\mu_0}{4\pi} \int \int \int \frac{3\vec{M}(\vec{r}') \cdot (\vec{r} - \vec{r}')}{|\vec{r} - \vec{r}'|^5} (\vec{r} - \vec{r}') - \frac{\vec{M}(\vec{r}')}{|\vec{r} - \vec{r}'|^3} d vol \quad (1)$$

$$\vec{J} = \vec{\nabla} \times \vec{M} \quad (2)$$

with the help of an Inverse Problem solver.

As an illustrative example of the methodology, we will use the field maps of the three simulated welds with $J_c^{GB}/J_c^G = 100\%$, 90% and 50% were obtained by using an Inverse Problem solver called ‘Caragol’ [22, 28]. This software program computes the critical current distribution in the sample, assuming: (i) that currents are planar, i.e., the J_z component perpendicular to the analysed surface is zero, and (ii) that J is homogeneous along the $z \parallel c$ direction. Further, no boundaries on the external shape of the sample have been considered. A user-friendly version of the software ‘Caragol’ is available on the Internet [27]. However, this online version resamples the submitted data before solving the Inverse Problem, inducing a loss of resolution in the final results. In order to skip that step, we used an improved version of this program based on a Fourier algorithm [26], allowing us to obtain an enhanced spatial resolution in the resulting current density maps.

As expected, the $J_y(x, y)$ map for the 100% case consists of two triangular zones where the current density is non-null and constant for each zone (figure 2(a), right). In the 90% case, the depression of the superconducting performance is appreciated by a slight deformation of the triangular zones, even though the values of the current density at the deformed zone remain high (figure 2(b), right). Finally, the computed current density map for the 50% case (figure 2(c), right) clearly shows the four triangular zones corresponding to the J_c^G component and the two central zones exhibiting lower current density values which correspond to the J_c^{GB} values.

3.3. Inter- and intra-granular critical current densities of actual welds

We will present next a method for the experimental determination of J_c^{GB} and J_c^G in real welded samples, based on the previous analysis.

In order to present the method, it is instructive to consider first the case of a low-quality joint. Figure 3(a) shows the typical Hall probe magnetization map in the remanence of such a weld. As expected, a reduction of the remanent magnetization along the junction can be observed.

The current density distribution can be calculated from the measured $B_z(x, y)$ map by back-solving the Biot–Savart law with the help of the software package ‘Caragol’ [22]. Figure 3(b) shows for instance the circulation of currents calculated from the magnetization map of figure 3(a). The

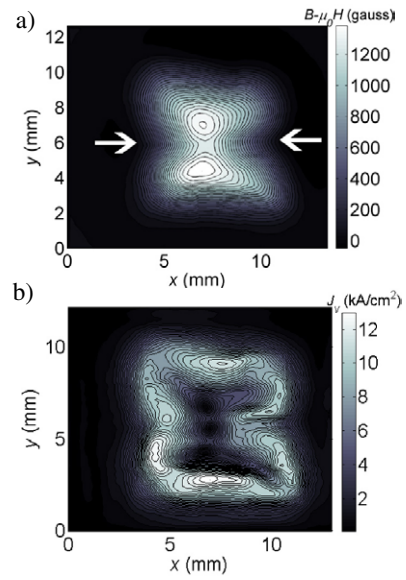


Figure 3. (a) Magnetization map for a welded sample where the junction shows lower trapped field compared to the rest of the material. The junction position is indicated by the white arrows. (b) Computed current density modulus $J_y(x, y)$ for the same sample.

current loop extending over the whole sample, and the two isolated intra-grain current loops, can be appreciated.

We will consider only the J_y component map for the determination method of J_c^{GB} and J_c^G , as illustrated in figure 4. It can be observed that the experimental results agree reasonably well with the theoretical pattern and the simulated example shown above in figure 2(c), right. The J_y pattern exhibits four triangle areas (a, b, c and d) and one rhomboidal area.

First, we trace two profiles parallel to the junction, one at each side of it, passing by those extreme values (figure 4, profiles 1 and 3). According to the Bean model, one would expect a profile formed by two plateaus (figure 1(b)). Experimentally we rather obtain two rounded peaks, with the critical current density strongly decreased at the sample borders and optimum at the centre of the grains.

Ideally, the value of the intra-grain critical current density at the four peaks would be the same. However, due to inhomogeneity of the original material and its impact over the current densities, the values obtained from each of the triangles do not coincide exactly; we will denote them as J_{ca}^G , J_{cb}^G , J_{cc}^G , J_{cd}^G . By tracing a profile perpendicular to the junction, at the position of any pair of peaks (figure 4, profile 4), we can observe a minimum which coincides with the position of the junction. Now we can trace a profile along the junction (figure 4, profile 2). The profile presents two peaks, corresponding to the inter-granular critical current density, J_c^{GB} . Again, for a homogeneous interface, the J_c^{GB} values at the two extremes would be the same, but this will not be the case in practical situations, where we will need to consider the two values J_{cf}^{GB} and J_{cg}^{GB} separately.

The J_c^{GB}/J_c^G ratio is a useful figure of merit to describe the quality of welds. In the case of inhomogeneous YBCO starting material, in order to obtain this ratio we will compare

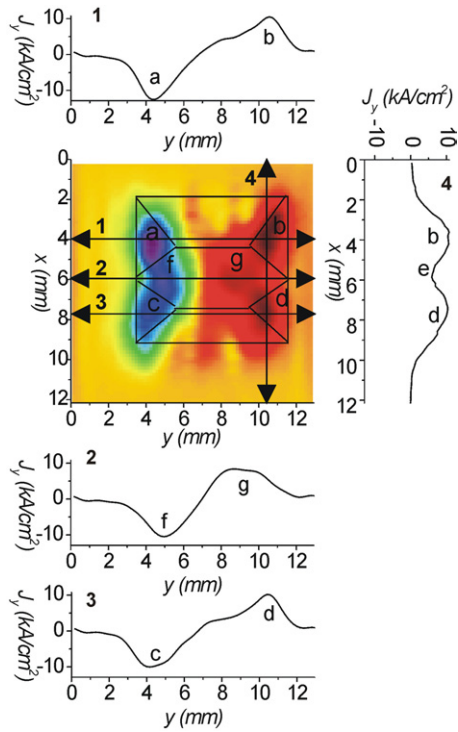


Figure 4. Schematic diagrams summarizing the method for the determination of the J_c^{GB} and J_c^G from the $J_y(x, y)$ critical current density component map in a low-quality welded sample. J_c^G is determined from peaks a and b, in profile number 1, and from peaks c and d in profile number 3. The position of the weld, which is marked as e, is found from profile 4. The J_c^{GB} value is determined from f and g in the profile on top of the joint, represented in profile 2.

the critical current density at the joint with the lowest of the two J_c^G intra-grain values at each side of the junction. That is, for each sample we will obtain two ratios: J_c^{GB} over the minimum of (J_{ca}^G, J_{cb}^G) , and J_c^{GB} over the minimum of (J_{cd}^G, J_{cb}^G) . This estimation is justified by the fact that the critical current density at the joint obtained by the welding process can be only similar or lower to the smallest intra-grain critical current density of the YBCO monoliths to be joined.

In the case of a very good-quality joint, the welded sample acts as a single domain and a different analysis has to be carried out, since the current distribution will show a different shape. Figure 5(a) shows the measured magnetization map for such a case. This map exhibits only one peak, indicating that the superconducting properties at the joint are not depressed. If the current density distribution is computed and the profile perpendicular to the junction is traced (see figure 5(b)), the values of the grain are comparable with the values of the grain boundary on the right-hand side of the map. On the left-hand side of the map, the profile shows its maximum value exactly on the junction. If the ratio J_c^{GB}/J_c^G is calculated for the values obtained at the right-hand side of the map (see figure 5(b), right), that is $J_c^{GB} = 14 \text{ kA cm}^{-2}$, $J_c^{G\min} = 15 \text{ kA cm}^{-2}$, a value of 93% is obtained. In contrast, if the ratio is calculated on the left-hand side (figure 5(b), left), since there is no relative minimum for the perpendicular profile on that side, the $J_c^{GB}/J_c^{G\min}$ ratio can be assumed to be one.

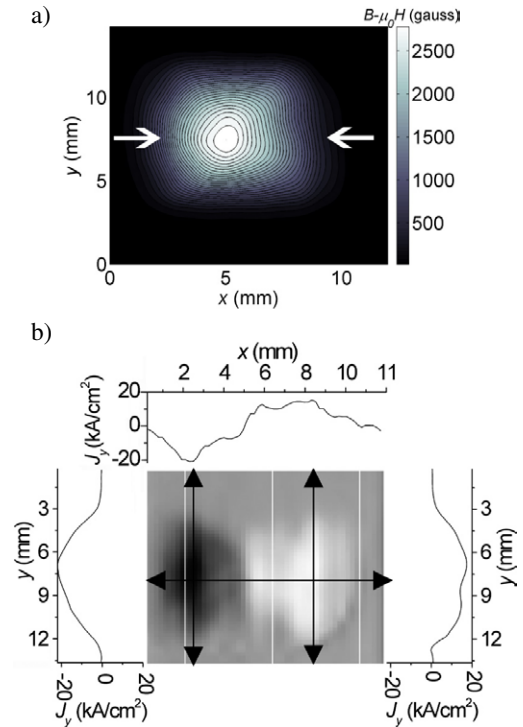


Figure 5. Characterization of a welded sample where the quality of the joint is similar to that of the grain. (a) Magnetization map (the position of the junction is indicated by the white arrows). (b) $J_y(x, y)$ map after solving the Inverse Problem.

4. Conclusions

We have developed a methodology for determining both inter- and intra-grain critical current densities in artificial superconducting welds.

The method is based on the interpretation of the current density patterns expected from the Bean model for a two-domain block. This method has enabled us to evaluate the quality of the samples welded by using an Ag-induced melting technique developed in our group.

The field profile was calculated from three different simulated current density distribution patterns exhibiting three different ratios in order to evaluate the influence of that ratio. It has been shown that the presence of two peaks in the trapped field map does not necessarily mean a failure of the welding process, since in many cases the critical current density ratios remain high. We have also reobtained the current distributions for each case and those distributions are in good agreement with the ones initially simulated.

It has also been shown that the value of current density flowing through the weld is dominated by the values of the current density circulating inside the grains. This proves that the quality of the joint can be as high as the quality of the starting material.

Acknowledgments

This work was supported by the EU-TMR network Supermachines RTN1-1999-00282, the projects MAT2002-02642 and MAT2003-01584, and Generalitat de Catalunya (Pla de Recerca 00206 and CeRMAE).

AP would like to acknowledge MEC for her doctorate fellowship. EB would like to thank the CSIC for her I3P post-doctoral fellowship.

References

- [1] Murakami M 1992 *Supercond. Sci. Technol.* **5** 185
- [2] Jee Y A, Kim C J, Sung T H and Hong G W 2000 *Supercond. Sci. Technol.* **13** 195
- [3] Kim C J, Kim H J, Jee Y A, Heng G W, Joo J H, Han S C, Han Y H, Sung T H and Kim S J 2000 *Physica C* **338** 205
- [4] Chen L H, Claus H, Paulikas A P, Zheng H and Veal B W 2002 *Supercond. Sci. Technol.* **15** 672
- [5] Salama K and Selvamanickam V 1992 *Appl. Phys. Lett.* **60** 898
- [6] Noudem J G, Reddy E S, Tarka M, Noe M and Schmitz G J 2001 *Supercond. Sci. Technol.* **14** 363
- [7] Walter H, Jooss C, Sandiumenge F, Bringmann B, Delamare M P, Leenders A and Freyhardt H C 2001 *Europhys. Lett.* **55** 100
- [8] Yoshioka J, Iida K, Negichi T, Sakai N, Noto K and Murakami M 2002 *Supercond. Sci. Technol.* **15** 712
- [9] Puig T, Rodriguez P, Carrillo A E, Obradors X, Zheng H, Welp U, Chen L, Claus H, Veal B W and Crabtree G W 2001 *Physica C* **363** 75
- [10] Harnois C, Desgardin G, Laffez I, Chaud X and Bourgault D 2002 *Physica C* **383** 269
- [11] Iliescu S, Granados X, Bartolomé E, Sena S, Carrillo A E, Puig T, Obradors X and Evetts J E 2004 *Supercond. Sci. Technol.* **17** 182
- [12] Iliescu S, Carrillo A E, Bartolomé E, Granados X, Bozzo B, Puig T, Obradors X, García I and Walter H 2004 *Supercond. Sci. Technol.* **18** 168
- [13] Doyle R A, Bradley A D, Lo W, Cardwell D A, Campbell A M, Vanderbemden P and Cloots R 1998 *Appl. Phys. Lett.* **73** 117
- [14] Claus H, Welp U, Zheng H, Chen L, Paulikas A P, Veal B W, Gray K E and Crabtree G W 2001 *Phys. Rev. B* **64** 14
- [15] Zheng H, Claus H, Chen L, Paulikas A P, Veal B W, Olsson B, Koshelev A, Hull J and Crabtree G W 2001 *Physica C* **350** 17
- [16] Surzhenko A B, Zeisberger M, Habisreuther T, Gawalek W and Uspenskaya L S 2003 *Phys. Rev. B* **68** 064504-1
- [17] Jooss C, Bringmann B, Walter H, Leenders A and Freyhardt H C 2000 *Physica C* **341** 1423
- [18] Jooss C, Albrecht J, Kuhn H, Leonhardt S and Kronmüller H 2002 *Rep. Prog. Phys.* **65** 651
- [19] Chikumoto N, Oishi M, Yoshioka J, Iida K and Murakami M 2003 *Physica C* **388** 413
- [20] Granados X, Sena S, Bartolomé E, Palau A, Puig T, Obradors X, Carrera M, Amorós J and Claus H 2003 *IEEE Trans. Appl. Supercond.* **13** 3667
- [21] Iliescu S, Sena S, Granados X, Bartolomé E, Puig T, Obradors X, Carrera M, Amorós J, Krakunovska S and Habisreuther T 2003 *IEEE Trans. Appl. Supercond.* **13** 3136
- [22] Carrera M, Amorós J, Obradors X and Fontcuberta J 2003 *Supercond. Sci. Technol.* **16** 1187
- [23] Ullrich M, Walter H, Leenders A and Freyhardt H C 1999 *Physica C* **311** 86
- [24] Bartolomé E, Granados X, Puig T, Obradors X, Reddy E S and Schmitz G J 2004 *Phys. Rev. B* **70** 144514
- [25] Bean C P 1962 *Phys. Rev. Lett.* **8** 250
- [26] Granados X, Bozzo B, Iliescu S, Bartolomé E, Puig T, Obradors X, Amorós J and Carrera M 2005 *IEEE Trans. Appl. Supercond.* **15** 3632
- [27] Bartolomé E, Gomory F, Granados X, Puig T and Obradors X 2005 *Supercond. Sci. Technol.* **18** 388
- [28] Amorós J, Carrera M, Iliescu S, Bozzo B, Granados X, Puig T and Obradors X 2005 *EUROSAS 2005 (11–15 September, Vienna, Austria)* submitted